JOURNAL OF SOLID STATE CHEMISTRY **136,** 313–319 (1998)
ARTICLE NO. SC977714

Metal–Insulator Transitions Induced by Doping in $LaNiO_3$: $LaNi_{0.95}M_{0.05}O_3$ (M = Mo, W, Sb, Ti, Cu, Zn) Perovskites

I. Álvarez,[1] M. L. Veiga, and C. Pico

Departemento de Química Inorgánica I, Facultad de Ciencias Químicas, Universidad Complutense, 28040 Madrid, Spain

Received June 23, 1997; in revised form November 14, 1997; accepted November 18, 1997

Structural characterization and electronic properties of the $LaNi_{0.95}M_{0.05}O_3$ (M = Mo, W, Sb, Ti, Cu, Zn) perovskite-like system are reported. These compounds can be regarded as being derived from $LaNiO_3$ by partial substitution of Ni^{3+} in this material by M^{6+}, M^{5+}, M^{4+}, or M^{2+} formal cations, with a partial reduction of Ni^{3+} to Ni^{2+} taking place. X-ray powder diffraction data were analyzed by means of the Rietveld method and show that all the title materials present perovskite-type structure with a rhombohedral (S.G. $R\bar{3}c$) or orthorhombic (S.G. *Pbnm*) symmetry, depending on the nature of the M cation. In all cases, Ni and M cations are placed at random in octahedral B-sites of perovskite structure. Electrical resistivity measurements (four probe method) show metal-to-insulator (M–I) transitions for M = Mo, W, Ti, Cu, Zn at temperatures of about 50 K and a semiconductor behavior for the Sb sample in the whole temperature range explored. Magnetic susceptibility measurements show the presence of weak ferromagnetic interactions for M = Sb and Pauli paramagnetism for the remaining compounds.

INTRODUCTION

Over the past several years, $LaNiO_3$ oxide, known to have a rhombohedrically distorted perovskite structure, and some derived systems have generated considerable interest. It has been shown that correlation effects are decisive in the magnetic (Pauli paramagnetism with Stoner enhancement) and electrical (correlated metal with a quadratic dependence between resistivity and temperature at low temperatures) behavior of this material (1, 2). In this context, some systems derived from $LaNiO_3$, such as $RNiO_3$ (R = rare earth) (3, 4), $LaNi_{1-x}M_xO_3$ (M = Cr, Mn, Fe, Co, Cu, Sb) (5–8), $R_{1-x}M_xNiO_3$ (M = Sr, Th) (9), $La_{n+1}Ni_nO_{3n+1}$ (10), and $A_xLa_{1-x}Ni_{1-y}M_yO_3$ (M = Fe, Cr, Co, Mn, W, Te) (11) have been extensively studied. In some of them, composition-, temperature-, and structure-driven M–I transitions have been reported. In the cases in which Ni cations are present in mixed-valent state, electrical and magnetic properties could be qualitatively related to the relative amounts of Ni^{2+} and Ni^{3+}, taking into account the probability of antiferro- or ferromagnetic interactions and the evolution of electronic localization in the systems. Therefore, both structural aspects and electronic correlation effects seem to be responsible for the observed behavior. We have previously reported structural and electronic results for the $LaNi_{1-x}W_xO_3$ system (12, 13) in which temperature- and composition-driven M–I transitions have been observed. Taking into account the composition effect, a M–I transition at $x > 0.10$ was found. On the other hand, for the less doped material, $x = 0.05$, a M–I transition governed by temperature was detected at about 50 K. In this work we concentrate in the doping of $LaNiO_3$ system in the perovskite B-sublattice with cations of different charges and sizes, maintaining the substitution degree of 5%. In this sense, our aim has been focused on the study of structural and electrical features of the title compounds, the comparison of results with those of the nondoped phase, and the establishment of the most important parameters which drive the observed physical phenomena.

EXPERIMENTAL

The $LaNi_{0.95}M_{0.05}O_3$(M = Mo, W, Sb, Ti, Cu, Zn) materials were prepared by the solgel method starting from stoichiometric amounts of $La(NO_3)_3 \cdot 6H_2O$, $Ni(NO_3)_2 \cdot 6H_2O$, WO_3, Sb_2O_3, TiO_2, $Cu(NO_3)_2 \cdot 3H_2O$ and $Zn(NO_3)_2 \cdot 4H_2O$ at temperatures ranging between 1173 and 1223 K for several days. The details of the synthesis method can be found in Ref. (6). During the thermal treatment, the samples were regrinded in each step and the process was monitored by X-ray powder diffraction until single phases were obtained. The X-ray diffraction patterns were recorded using a Philips X'Pert MPD diffractometer with a D-5000 (3051/00) goniometer. A step scan of 0.04 and a counting time of 15 s per step were employed. The goniometer was connected to a PC controlled by the commercial program PC-APD (Analytical Powder Diffraction Software, 4.0). The

[1]To whom correspondence should be addressed.

0022-4596/98 $25.00

TABLE 1
Ni^{3+} Concentration and Stoichiometry of the Title Compounds

Comp., *M*	z^a	0.95-z^a	Stoichiometry
Ti	0.86	0.09	$LaNi_{0.94}Ti_{0.05}O_{2.96}$
Cu	0.92	0.03	$LaNi_{0.95}Cu_{0.05}O_{2.96}$
Zn	0.92	0.03	$LaNi_{0.95}Zn_{0.05}O_{2.96}$

[a] z is the Ni^{3+} percentage per one and (0.95-z) is the Ni^{2+} percentage per one.

TABLE 2
Crystal Data and *R* factors for $LaNi_{0.95}Zn_{0.05}O_3$

Atom	Position	*x*	*y*	*z*
La	6*a*	0	0	0.25
Ni/Zn	6*b*	0	0	0
O	18*d*	− 0.543(2)	0	0.25

$a = 5.458(1)$ (Å) $c = 13.165(1)$ (Å) space group = $R\bar{3}c$ (No. 167)
$R_p = 11.8$ $R_{wp} = 15.5$ $R_B = 8.4$ $\chi^2 = 8.8$

data were analyzed by the Rietveld method by means of the Fullprof program (14).

For the electronic resistivity measurements, pelletized samples were sintered at temperatures somewhat lower than the respective synthesis temperatures in order to assure the thermal stability of the sample. Pycnometric measurements showed that, for all the samples, the densities were greater than 90% of the crystallographic values. Electronic resistivity was measured using the Van der Pauw method (15), which avoids the contact effects. Contacts were made by covering the circular faces of the sample pellets with platinum paint.

The magnetic susceptibility measurements were done using a DSM8 pendulum susceptometer based on the Faraday method. The maximum applied magnetic field was 15 kG with $H(dH/dz) = 29\,kG^2 \cdot cm^{-1}$. The equipment was calibrated with $Hg(Co(SCN)_4)$ and $Gd_2(SO_4)_3 \cdot 8H_2O$, with χ independent of the field in the temperature range of measurements. The magnetic susceptibility data have been corrected taking into account the ionic diamagnetic contribution from
Ref. (16).

RESULTS AND DISCUSSION

1. Compositional and Structural Characterizations

Table 1 shows the Ni^{3+} concentration and stoichiometry for some of the title compounds obtained by iodometric titration. In general, good agreement between the expected and the observed oxygen contents can be observed.

X-ray diffraction data for the title compounds were analyzed by means of the Rietveld method and they show a perovskite-type structure for all compounds. However, the observed symmetry is rhombohedral (S.G. $R\bar{3}c$) for M = Ti, Cu, Zn, while the M = Mo, W, Sb samples show an orthorhombic symmetry. As an example, Fig. 1 shows the ob-

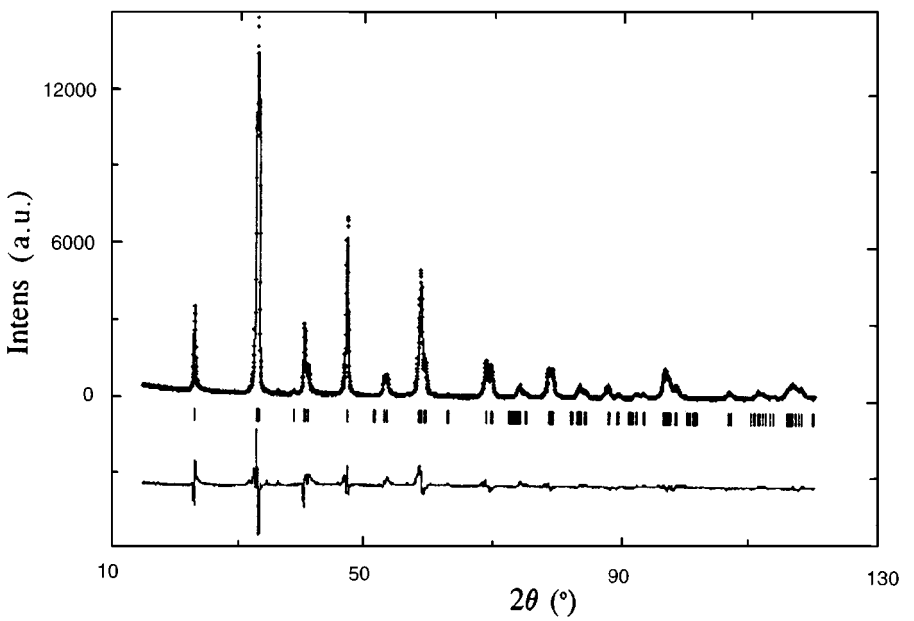

FIG. 1. Observed (dotted line), calculated (solid line), and difference (vertical marks) X-ray diffraction profiles for $LaNi_{0.95}Zn_{0.05}O_3$.

TABLE 3
Bond Distances (Å) for $LaNi_{0.95}Zn_{0.05}O_3$

La–O	2.96(1)	(Ni/Zn)–O	1.934(1) × 2
	2.49(1)		1.934(8) × 2
	2.964(5) × 2		1.934(7) × 2
	2.493(5) × 2	Mean	1.934
	2.711(1) × 2	Shannon	1.96
	2.711(5) × 2		
	2.711(6) × 2		
Mean	2.72		
Shannon	2.76		

served and calculated X-ray diffraction profiles and the difference between them and the allowed reflections for the rhombohedral phase with $M = Zn$. The crystallographic data for the orthorhombic oxides can be found elsewhere (12). In Table 2 the crystal data and the R-factors obtained in this refinement are gathered. The agreement of the profiles and the R-factors obtained seem to confirm the validity of the proposed structural model. The most representative bond lengths for the Zn compound are given in Table 3. The mean values and the sums of the Shannon ionic radii (17) are also included and, as can be observed, they agree reasonably.

The results showing the evolution of cell parameters and cell volume for the $LaNi_{0.95}M_{0.05}O_3$ mixed oxides are compiled in Table 4. The evolution of these crystal parameters and the adoption of rhombohedral or orthorhombic symmetry can be explained taking into account charge and size parameters of each cation involved, and these features are compiled in the Goldschmidt factor (18), t ($t = d(A–O)/\sqrt{2}\cdot d(B–O)$, where $d(A–O)$ and $d(B–O)$ are the bond lengths between cations in the A or B sublattice, respectively, and the oxygen anions. This t factor has been used extensively to explain and predict the adopted symmetry in materials with perovskite-type structure. Table 5 shows the t values for the title materials, obtained taking into account the stoichiometries found from chemical analysis and ionic

TABLE 4
Cell Parameters and Cell Volume for $LaNi_{0.95}M_{0.05}O_3$

M	a (A)	b (A)	c (A)	V (A^3)
W	5.419(2)	5.494(2)	7.699(4)	229.2
Mo	5.451(4)	5.471(2)	7.752(5)	231.2
Sb	5.403(4)	5.483(1)	7.750(1)	229.6
—[a]	5.446(1)		13.154(1)	338.1
Ti	5.451(1)		13.149(1)	338.3
Cu	5.437(1)		13.085(1)	335.0
Zn	5.458(1)		13.165(1)	339.6

[a] Values for the reference sample, $LaNiO_3$.

TABLE 5
***t* Values and Mean Size of *M*/Ni Cations for the Title Oxides**

Compound	r_{mean} (Å)[a]	t[b]
$LaNiO_3$	0.56	0.996
$LaNi^{3+}_{0.92}Ni^{2+}_{0.03}Zn^{2+}_{0.05}O_{2.96}$	0.573	0.989
$LaNi^{3+}_{0.92}Ni^{2+}_{0.03}Cu^{2+}_{0.05}O_{2.96}$	0.572	0.989
$LaNi^{3+}_{0.85}Ni^{2+}_{0.10}Ti^{4+}_{0.05}O_{2.97}$	0.575	0.988
$LaNi^{3+}_{0.80}Ni^{2+}_{0.15}W^{6+}_{0.05}O_3$	0.581	0.985
$LaNi^{3+}_{0.78}Ni^{2+}_{0.17}Mo^{6+}_{0.05}O_{2.99}$	0.581	0.985
$LaNi^{3+}_{0.77}Ni^{2+}_{0.18}Sb^{5+}_{0.05}O_{2.96}$	0.585	0.983
$NdNiO_3$	0.56	0.963

[a] Mean values of ionic radii for cations located at B-sites of perovskite structure.

[b] Values obtained considering coordination XII for the La^{3+} cation.

radii from Shannon (17). The corresponding values for $LaNiO_3$ (rhombohedral) and $NdNiO_3$ (orthorhombic) are included for clarity in understanding the present data. As can be observed, the limit value of t which drives the adoption of rhombohedral-vs-orthorhombic symmetry seems to be 0.988. On the other hand, the cell-volume data in Table 4 are in good agreement with the mean sizes of the cations concerned in each case.

In summary, from the above structural results, we can conclude that $LaNi_{0.95}M_{0.05}O_3$ compounds have perovskite-type structures with rhombohedral or orthorhombic symmetry in which both Ni and M cations are placed at random in the octahedral B-sites.

2. *Conductivity Measurements*

The electronic conductivity variation with temperature for the $LaNi_{0.95}M_{0.05}O_3$ mixed oxides has been measured in the 5–300 K temperature range (in some cases the

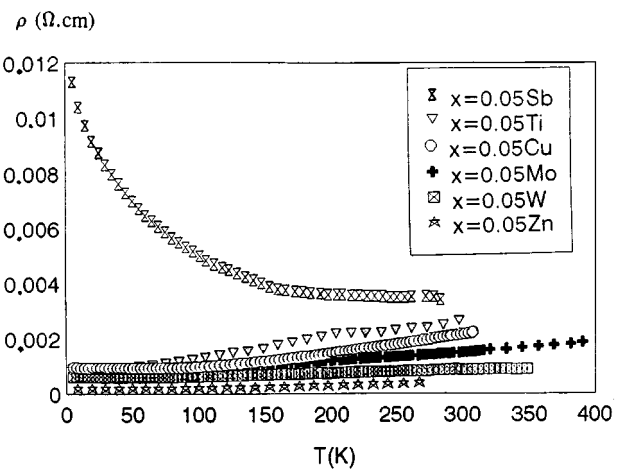

FIG. 2. Resistivity variation with temperature for $LaNi_{1-x}M_xO_3$.

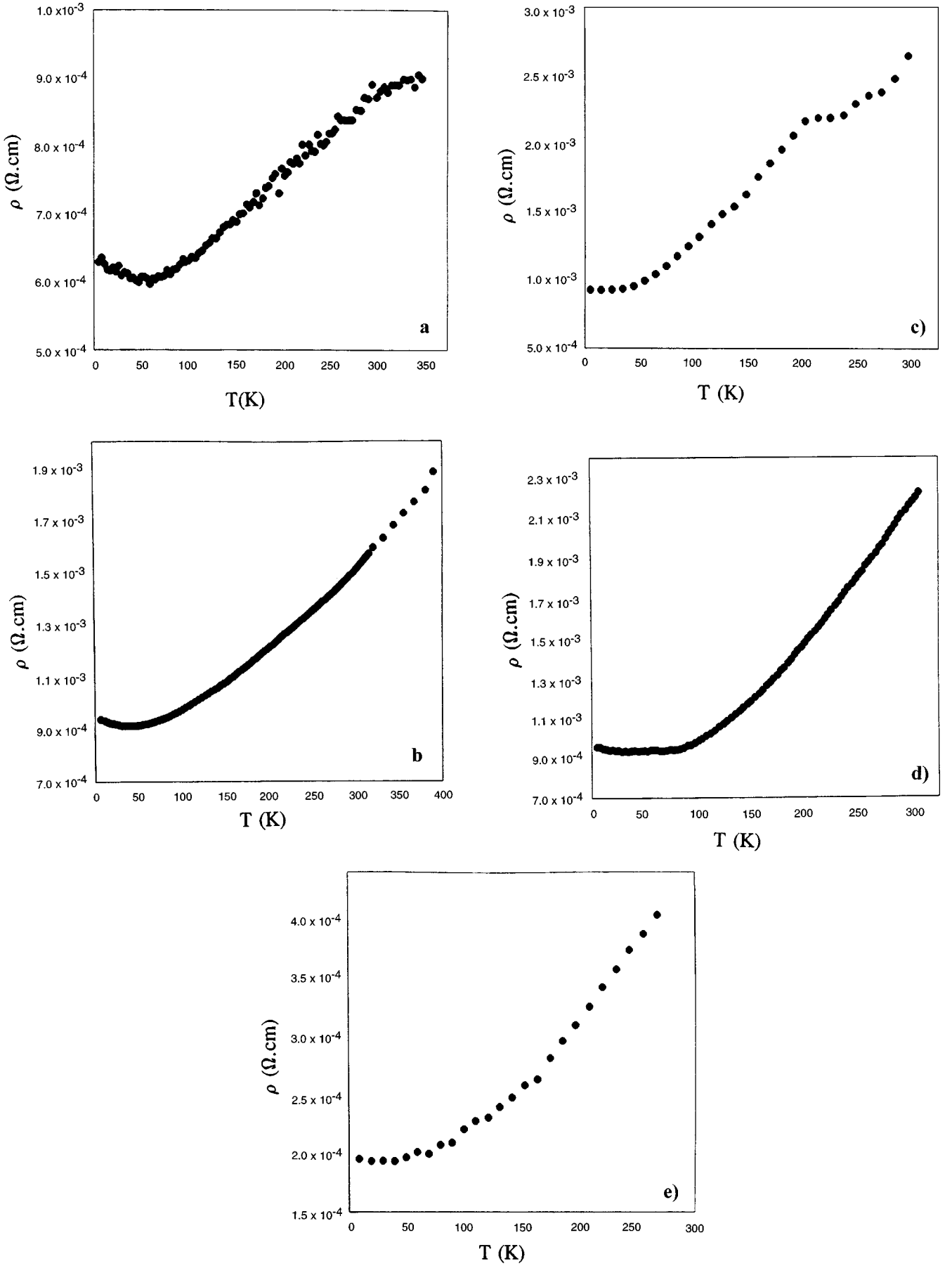

FIG. 3. Resistivity variation with temperature for M = (a) W, (b) Mo, (c) Ti, (d) Cu, and (e) Zn.

TABLE 6
Fit Parameters Following Eq. [1] for $LaNi_{0.95}M_{0.05}O_3$

Comp.	ρ_o (m$\Omega\cdot$cm)	B (m$\Omega\cdot$cm/K)	A (m$\Omega\cdot$cm/K^2)	DT[a]	r^2[b]
$LaNiO_3$	0.5	0	0.034	4.2–55	—
M = W	0.6	− 0.2	0.006	50–150	0.991
M = Mo	0.9	0.3	0.007	50–200	0.999
M = Ti	0.9	− 2.0	0.050	5–55	0.988
M = Cu	1.1	− 4.0	0.040	60–140	0.998
M = Zn	0.2	− 0.1	0.004	5–150	0.989

[a] Temperature range considered in the fit.
[b] r-factor expressing the goodness of the regression (ideally equal to 1).

temperature region explored has been extended to 400 K by the four probe method. Fig. 2 shows the resistivity variation with temperature for the title compounds. It can be deduced from this graph that all these oxides except the Sb-containing one behave as metals, *i.e.*, resistivity increases when temperature is increased. As has been reported earlier (11), the observed behavior in the Sb compound could be explained as a consequence of the electronic features of this cation: the absence of *d*-orbitals can provoke the frustration of metallic properties, *i.e.*, the orbital overlapping is less effective when orbitals with very different symmetry and

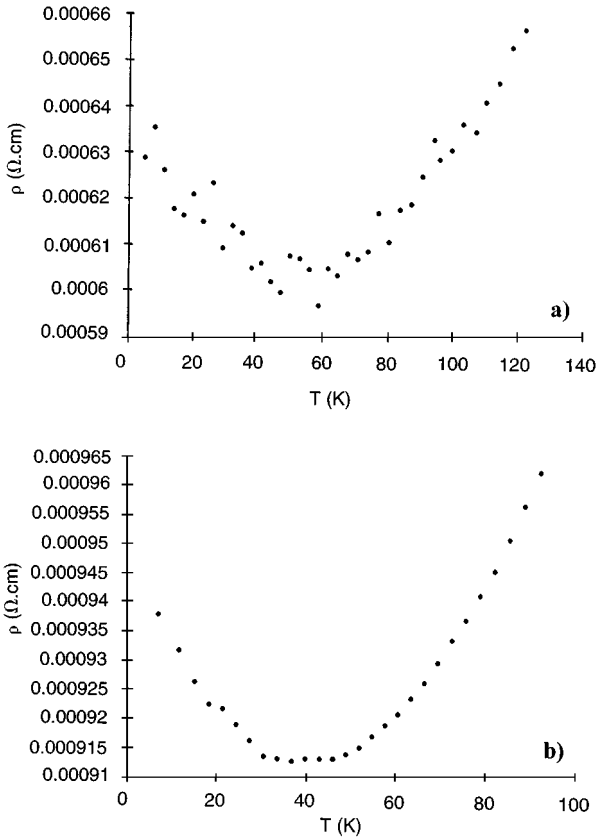

FIG. 5. M–I transition for (a) M = W and (b) M = Mo.

energy are concerned, and this gives rise to narrower bands or localized levels, which prevent the stabilization of metallic properties.

To demonstrate in detail the resistivity variation with temperature for the metallic phases, Fig. 3 shows the graphs corresponding to M = W, Mo, Ti, Cu, Zn. It can be observed that this variation deviates from linearity below

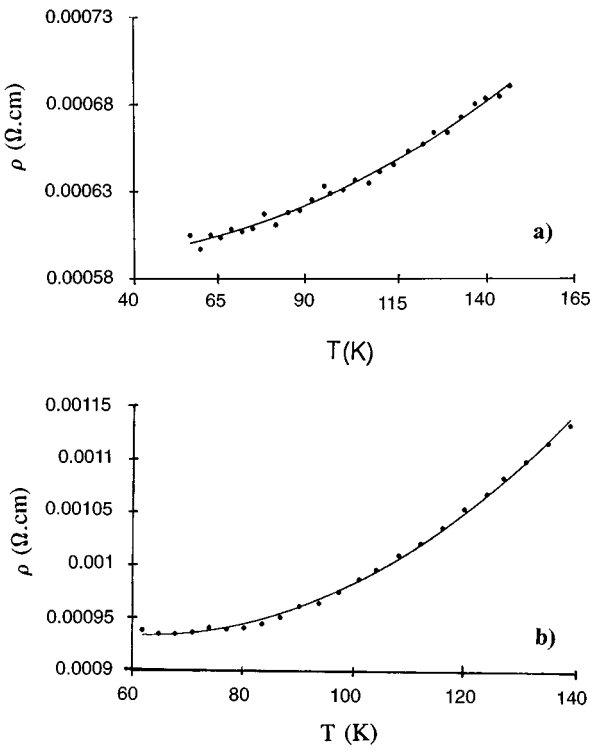

FIG. 4. Experimental and calculated (from Eq. [1]) resistivity vs temperature data for (a) M = W and (b) M = Cu.

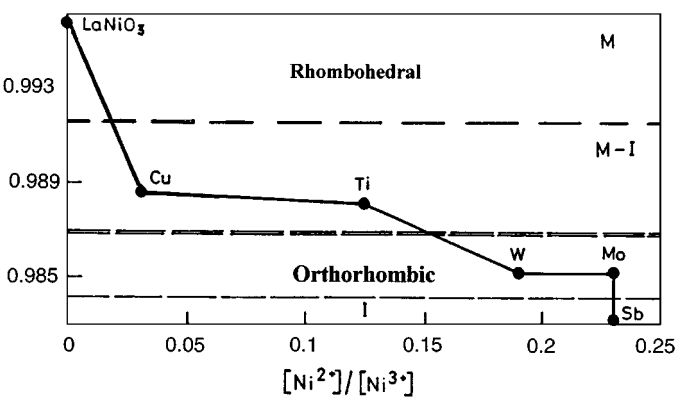

FIG. 6. Dependence of t with Ni^{3+} and Ni^{2+} relative concentrations.

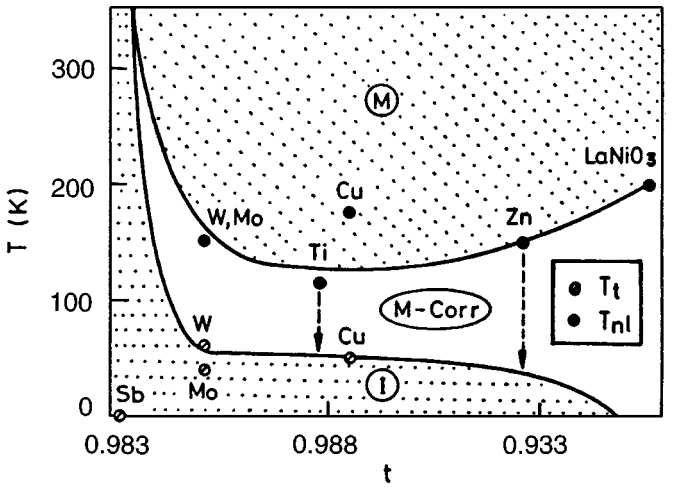

FIG. 7. Variation of T_t and T_{nl} (see text) with t.

a certain temperature ranging between 200 and 125 K, depending on the sample. This behavior is similar to that found for the $LaNiO_3$ material, for which a quadratic dependence below 55 K has been established. This fact has previously been attributed to important electronic correlations between $3d$ electrons in a quarter-filled e_g-type band (2, 3). In this sense, $LaNi_{0.95}M_{0.05}O_3$ mixed oxides show a similar behavior at higher temperatures whereas at low temperatures metal–insulator transitions (M–I), which can be related to the increase in electronic correlations as a consequence of doping, are detected.

The experimental data fit, in different temperature ranges depending on the sample, the following equation:

$$\rho(T) = \rho_0 + B \cdot T + A \cdot T^2. \qquad [1]$$

Table 6 shows the obtained parameters for every fit and the temperature range considered in each case. It can be observed that the obtained values for the constants ρ_0, A, and B are of the same order as those of the $LaNiO_3$ phase. As representative example, Figs. 4a and 4b show the experimental and calculated data from the fit for the W and Cu phases respectively; at still lower temperatures, a M–I transition is observed, as illustrated in Figs. 5a and 5b for the W and Mo phases, respectively. These results can be explained in terms of the electronic localization present in each case as a function of (i) structural parameters related to the respective Ni^{3+}/Ni^{2+} concentrations and summarized in the t factor, and (ii) the temperature. Let us analyze each feature in turn.

TABLE 7
T_t, T_{nl}, and t Values (See Text) for $LaNi_{0.95}M_{0.05}O_3$

Compound	t	T_t (K)	T_{nl} (K)
$LaNiO_3$	0.996	—	~ 200
M = W	0.985	~ 60	~ 150
M = Mo	0.985	~ 40	~ 150
M = Sb	0.983	—	—
M = Ti	0.988	—	~ 125
M = Cu	0.989	~ 50	~ 175
M = Zn	0.993	—	~ 150

(i) Figure 6 shows the dependence of the tolerance factor t (as described above) with Ni^{3+} and Ni^{2+} relative concentrations. Having in mind the band model proposed for $RNiO_3$ (3) and $LaNi_{1-x}W_xO_3$ (13), in which the electrical behavior is driven by the parameters W (band width) and Δ (energy difference between oxygen $2p$ orbitals and metallic empty $3d$ orbitals), it seems that in the $LaNi_{0.95}M_{0.05}O_3$ system, W significantly decreases as Ni^{2+} concentration increases and t becomes lower, at least at the temperature range explored. The limit values of both parameters are $[Ni^{2+}]/[Ni^{3+}] = 0.03$ and $t = 0.994$. For lower Ni^{2+} concentrations and higher t values, metallic behavior is observed (this is the case of the not-doped sample, $LaNiO_3$), whereas for the opposite case, M–I transitions are obtained. Finally, for $[Ni^{2+}]/[Ni^{3+}] \sim 0.25$ and $t < 0.983$, semiconductor behavior is obtained in the whole temperature range explored (this is the case of the Sb compound).

(ii) Figure 7 shows the variation of two important temperature parameters, T_t (M–I transition temperature) and T_{nl}, (below which a nonlinear variation of resistivity with temperature is observed) with the tolerance factor t. These temperatures are gathered in Table 7 for clarity. It can be observed that all materials behave as metallic above 125 K for any t value, *i.e.*, for any symmetry. At limit t values, unequivocal behavior is obtained: for $t \sim 0.983$ (M = Sb) only an I (insulator) behavior is detected, while for $t \sim 0.996$ ($LaNiO_3$), metallicity is observed. The remaining phases show M–I transitions as a function of temperature, as has been evidenced in the Mo, W, and Cu samples. For the Ti and Zn phases, a similar behavior, could be expected, but the experimental data registered over wide temperature ranges do not allow definitive conclusions in this respect (such a possibility is indicated in Fig. 7 by discontinuous lines).

In contrast, Fig. 8 shows the variation of molar magnetic susceptibility vs temperature for the title materials between 4.2 and 300 K. The M^{2+}-doped samples (with Cu and Zn) present a behavior different than that obtained for the Sb and W phases. In the Sb and W oxides, magnetic susceptibility is practically independent of temperature above ~80 and 150 K, respectively. Below these points, a marked increase is observed and could be interpreted considering ferromagnetic interactions, as discussed in the literature (19, 20). The Cu and Zn samples behave practically as $LaNiO_3$. For these materials, Pauli susceptibilities at 300 K of 4.1×10^{-4}, 4.8×10^{-4}, and 5.1×10^{-4}, emu·mol^{-1},

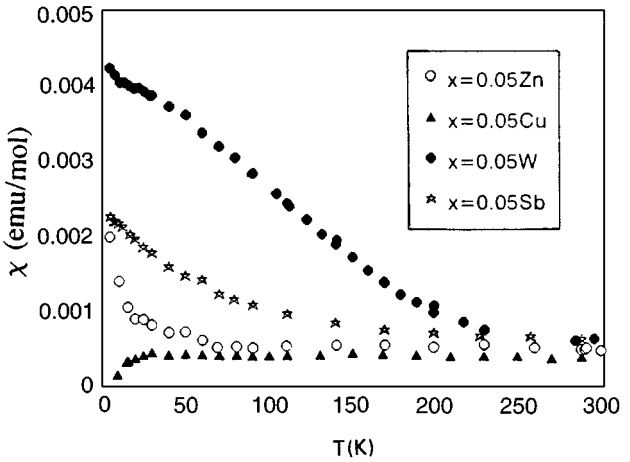

FIG. 8. Molar magnetic susceptibility vs temperature for $LaNi_{1-x}M_xO_3$.

respectively, are found. These results indicate that magnetic properties of the reference material, $LaNiO_3$, are not changed by the doping with 5% of Cu or Zn.

However, at temperatures below ~ 50 K (thus below T_t), magnetic susceptibility for $LaNi_{0.95}Cu_{0.05}O_3$ varies anomalously with temperature: χ_m values tend to zero at very low temperatures. Taking into account the obtained resistivity data, the possibility of superconductor behavior can be neglected. In this sense, the observed response can be explained in relation to the presence of small amounts of the extensively studied La_2CuO_4 (2l), which shows a superconductor property below ~ 50 K (depending on the oxygen content).

In summary, the magnetic behavior shown by the title materials is probably related to a limit value of $[Ni^{2+}]/[Ni^{3+}]$, which would drive the probability of antiferro- or ferromagnetic interactions. In this sense, it seems that below this value, magnetic interactions are not present or not detected.

ACKNOWLEDGMENT

We thank the CICYT (Property MAT 97-0326-C04-03, Spain) for financial support.

REFERENCES

1. K. P. Rajeev, G. V. Shivashankar, and A. K. Raychaudhuri, *Solid State Comm.* **79,** 7 (1991).
2. K. Sreedhar, J. M. Honig, M. Darwin, M. McElfresh, P. M. Shand, J. Xu, B. C. Crooker, and J. Spalek, *Phys. Rev. B* **46,** 10 (1992).
3. P. Lacorre, J. B. Torrance, J. Pannetier, A. I. Nazzal, P. W. Wang, and T. C. Huang, *J. Solid State Chem.* **91,** 225 (1991).
4. J. B. Torrance, P. Lacorre, A. I. Nazzal, E. J. Ansaldo and Ch. Niedermayer, *Phys. Rev. B* **45** 14, 8209 (1992). See also references therein.
5. Z. Zhang and M. Greenblatt, *J. Solid State Chem.* **111,** 145 (1994).
6. I. Álvarez, M. L. Veiga, and C. Pico, *Solid State Ionics* **91,** 265 (1996).
7. C. N. R. Rao, OM Parkash, and P. Ganguly, *J. Solid State Chem.* **15,** 186 (1975).
8. N. Y. Vasanthacharya, P. Ganguly, J. B. Goodenough, and C. N. R. Rao, *J. Phys. C*: *Solid State Phys.* **17,** 2745 (1984).
9. J. A. Alonso, M. J. Martínez-Lope, and M. Hidalgo, *J. Solid State Chem.* **116,** 146 (1995).
10. K. Sreedhar and J. M. Honig, *J. Sol. State Chem.* **111,** 147 (1994).
11. I. Álvarez, M. L. Veiga, and C. Pico, *Solid State Ionics* **93,** 329 (1997).
12. I. Álvarez, M. L. Veiga, and C. Pico, *J. Mater. Chem.* **5,** 1049 (1995).
13. I. Álvarez, J. L. Martínez, M. L. Veiga, and C. Pico, *J. Solid State Chem.* **125,** 47 (1996).
14. J. Rodríguez-Carvajal. Fullprof: A Program for Rietveld refinement and pattern matching analysis. Abstracts of Satellite Meeting on Powder Diffraction of XVth Congress of International Union of Crystallography, p. 127. Toulouse, 1990 (revised version, 1994).
15. L. J. Van der Pauw, *Philips Research Rep.* **1,** 13 (1958).
16. L. N. Mulay and E. A. Boudreaux (Eds.), "Theory and Applications of Molecular Paramagnetism," p. 494. Wiley, New York, 1976.
17. R. D. Shannon, *Acta Crystallogr. Sect. A* **32,** 751 (1976).
18. Goldschmidt, *Metallurgia* **62,** 241 (1960).
19. I. Álvarez, M. T. Fernández-Díaz, J. L. Martínez, M. L. Veiga, and C. Pico, *J. Solid State Chem.* (1997), in press.
20. I. Álvarez, M. L. Veiga, and C. Pico, *J. Alloys Compd.* (1997), in press.
21. P. A. Cox, "Transition Metal Oxides: an Introduction to their structure and properties." Clarendon Press, Oxford, 1992.